Optical measurements of charge-carrier mobilities in photorefractive sillenite crystals

Gilles Pauliat, Jean-Claude Launay, Gérald Roosen

Optical measurements of charge-carrier mobilities in photorefractive sillenite crystals

G. Pauliat and A. Villing

Institut d'Optique Théorique et Appliquée, Unité Associée au Centre National de la Recherche Scientifique, Centre Universitaire d'Orsay, B.P. 147, 91403 Orsay Cedex, France

J. C. Launay

Laboratoire de Chimie du Solide du Centre National de la Recherche Scientifique, 33405 Talence Cedex, France

G. Roosen

Institut d'Optique Théorique et Appliquée, Unité Associée au Centre National de la Recherche Scientifique, Centre Universitaire d'Orsay, B.P. 147, 91403 Orsay Cedex, France

Received October 2, 1989; accepted February 15, 1990

Analyses of the kinetics and magnitude of enhanced two-wave mixing gain under externally applied square-wave and sinusoidal electric fields are used to determine photocarrier drift mobility. These direct measurements do not require that any other photorefractive parameters be known.

INTRODUCTION

Photorefractive crystals exhibit large optical nonlinearities[1] and have great potential in optical data processing.[2] The extrinsic photorefractive effect in these electro-optic and photoconductive materials is rather well understood. The band-transport model[3] has been successfully employed to describe photorefraction in crystals such as the sillenite compounds, $Bi_{12}SiO_{20}$ and $Bi_{12}GeO_{20}$ (BGO).[4] The photorefractive effect results from photoexcitation of charge carriers in the conduction or valence band, followed by their migration and their final recombination in deep traps. An electric field is thus created, leading to an induced index pattern resulting from the electro-optic effect. This band-transport model has been employed to measure[5,6] the main photorefractive parameters[3]:

- N_A, the deep trap density,
- L, the diffusion length of charge carriers in the conduction or valence band,
- τ_{DI}, the dielectric relaxation time.

Knowledge of these parameters is of first importance because it permits the prediction of the kinetics of the photorefractive index modulation. However, the usual measurements are lengthy, and even careful precautions during the experiments do not prevent large uncertainties. Therefore it appears necessary to find a simpler way to determine the parameters.

We describe two methods of measuring with good accuracy the charge-carrier mobility μ, which is directly related to the diffusion length L and to the charge-carrier recombination time τ_R by[3]

$$L = \left(\frac{k_B T}{e}\mu\tau_R\right)^{1/2}, \tag{1}$$

where k_B is Boltzmann's constant, T is the temperature, and e is the charge on the carrier.

The recombination time τ_R can easily be determined from photocurrent measurements, and, therefore, the diffusion length L can be deduced from the mobility measurement. Furthermore, comparison between the values for the diffusion lengths found by conventional techniques and these new ones can confirm the validity of the band-transport model in the photorefractive samples.

The mobility measurement is based on the fact that a photorefractive grating consists of a superposition of an ionic grating and a charge-carrier grating. By a sudden and large change in the magnitude of an externally applied electric field we can shift the photocarrier grating while the ionic modulation (resulting from photoionization and charge-carrier recombination) remains unchanged for a short time. The charge-carrier grating shift is directly related to the charge-carrier velocity (e.g., to the mobility), and its effect on the total space-charge field can be observed by two-beam coupling experiments, for instance.

We first observed this effect while performing a two-beam-coupling experiment under a sinusoidal alternating electric field. For a given value of the ac field frequency we observed an unexpected reinforcement of the enhanced photorefractive gain. From this reinforcement we deduced the present methods. As we derived only approximate equations to calculate the mobility values with the sinusoidal field method, we will first explain how to deduce the mobility from the study of the kinetics of the gain by using the second method with square-wave applied fields. We will then experimentally check that the sinusoidal field method gives the same results.

We first use a band-transport model to find the optimum experimental conditions. However, we will demon-

0740-3224/90/081481-06$02.00

strate that the phenomenon that we observe does not depend on any model.

MATHEMATICAL ANALYSIS

We base our mathematical approach on the band-transport model, and we take into account one kind of charge carrier only (either electrons or holes). We rely on the analysis performed in the quasi-continuous regime by Valley.[7] In this development, the crystal is assumed to be illuminated by a sinusoidal irradiance pattern resulting from the interference of two coherent optical beams. Assuming that the interference pattern modulation index is low compared with unity and that the applied electric field E_0 is constant, a second time-derivative equation is found for the space-charge electric field δE:

$$\frac{\partial^2 \delta E}{\partial t^2} + \left(\frac{1}{\tau_a} + \frac{1}{\tau_b}\right)\frac{\partial \delta E}{\partial t} + \frac{1}{\tau_a}\frac{1}{\tau_b}(\delta E - E_{SC}) = 0, \quad (2)$$

where E_{SC} is the steady-state space-charge field and τ_a and τ_b are two complex constants whose expressions are given in Ref. 7. τ_b is proportional to the inverse of optical irradiance, so during the experiments this irradiance will be chosen low enough so that the imaginary part (or the real part) of $1/\tau_a$ is much larger than both the imaginary and the real parts of $1/\tau_b$. As is shown below, this condition is necessary for isolation of a term that is dependent only on the mobility. Equation (2) can be rewritten as

$$\frac{\partial^2 \delta E}{\partial t^2} + \frac{1}{\tau_a}\left[\frac{\partial \delta E}{\partial t} + \frac{1}{\tau_b}(\delta E - E_{SC})\right] = 0. \quad (3)$$

For low irradiance, the time constant τ_a is equal to

$$\frac{1}{\tau_a} = \frac{i}{\tau_E} + \frac{1}{\tau_R} + \frac{1}{\tau_{DI}} + \frac{1}{\tau_D}, \quad (4)$$

in which i represents the square root of -1, τ_E is the drift time constant, and τ_D is the diffusion time constant:

$$\tau_E = \frac{1}{k\mu E_0}, \quad (5)$$

$$\tau_D = \frac{e}{\mu k_B T k^2}, \quad (6)$$

with E_0 the external applied electric field, $k = 2\pi/\Lambda$ the grating wave number, and Λ the fringe spacing.

From Eq. (2) the kinetics of δE is described by

$$\delta E(t) = A \exp[-(t/\tau_a)] + B \exp[-(t/\tau_b)] + E_{SC}, \quad (7)$$

where the two constants A and B depend on the initial conditions at time $t = 0$. From Eqs. (4) and (7) we see that δE presents a fast oscillating behavior whose frequency is dependent only on the unknown mobility and on two other experimental parameters: the fringe spacing and the applied electric field. The mobility can thus be directly deduced from the study of the kinetics of δE. We will now pursue our analysis in order to optimize the experimental conditions necessary for easy observation of the oscillations.

First, we want to point out that δE given by Eq. (7) represents the space-charge field arising from both the ionic modulation δE^i and the charge-carrier modulation δE^{cc}:

$$\delta E = \delta E^i + \delta E^{cc}. \quad (8)$$

Using the development of Ref. 7, we derive the kinetics of the charge-carrier electric field. We get

$$\delta E^{cc}(t) = R\left\{A\left(1 - \frac{\tau_{DI}}{\tau_a}\right)\exp[-(t/\tau_a)] + B\left(1 - \frac{\tau_{DI}}{\tau_b}\right)\exp[-(t/\tau_b)] + E_{SC}\right\}, \quad (9)$$

with

$$R = -\frac{1}{\frac{\tau_{DI}}{\tau_D} + i\frac{\tau_{DI}}{\tau_E}}. \quad (10)$$

Coefficients A and B can now be calculated from the continuity conditions at $t = 0$. It should be noted that the first time derivative, $\partial\delta E/\partial t$, is not always continuous (for instance when the applied electric field is discontinuous), while δE^{cc} and δE^i (or δE) corresponding to physical quantities are always continuous.

Our purpose here is to perform an accurate measurement of the damped oscillations of δE caused by the fast time constant τ_a (e.g., τ_E). Therefore the imaginary part of $1/\tau_a$ (e.g., the oscillation pulsation $1/\tau_E$) must be larger than its real part (e.g., $1/\tau_D + 1/\tau_{DI} + 1/\tau_R$). The experiments thus have to be conducted with large fringe spacings and low irradiance to reduce both $1/\tau_D$ and $1/\tau_{DI}$. The applied electric field must also be large enough that the recombination time τ_R is larger than the drift time τ_E. Also, the amplitude of the damped oscillations must not be negligible compared with the overall signal. This condition is more difficult to fulfill. For instance, the response of the system to a modulation step:

$$\begin{cases} t < 0 & m = 0 \\ t > 0 & m \neq 0 \end{cases} \quad \text{or} \quad \begin{cases} t < 0 & m \neq 0 \\ t > 0 & m = 0 \end{cases} \quad (11)$$

will cause the ratio A/B to be equal to

$$\frac{A}{B} = -\frac{\tau_a}{\tau_b}. \quad (12)$$

Thus the two conditions $\|\tau_a\| \ll \|\tau_b\|$ and A not negligible compared with B contradict each other. A similar result is obtained when an external electric field step is applied to the crystal. Assuming that $\tau_E \ll \tau_R, \tau_D, \tau_{DI}$, we get

$$\begin{cases} t < 0 & E_0 = 0 \\ t > 0 & E_0 \neq 0 \end{cases} \Rightarrow \frac{A}{B} \simeq \frac{\tau_a}{\tau_{DI}}. \quad (13)$$

The physical reason for Eq. (12) [relation (13)] is that for $t < 0$ the photorefractive index modulation does not exist (is quite small) and reaches its steady state after a time $t \gtrsim \tau_b$. Therefore the amplitude of the space-charge field for $t \simeq \tau_a \ll \tau_b$ is negligible compared with its steady-state value. This is also the reason why the fast time constant τ_a is generally omitted in the usual analyses[3] with continuous optical beams.

In order to measure τ_a we have to break the relation given by Eq. (12). According to the above discussion, this is possible only if for the two sets of experimental conditions (for $t < 0$ and $t > 0$) we have δE large. For this reason we use the alternating field enhancement technique,[8,9] for which we will experimentally demonstrate that A/B is large enough to permit accurate measurements to be performed.

EXPERIMENTS

Two-beam coupling experiments in sillenite crystals are performed with the usual coupling configuration. The two coherent optical plane waves from an Ar^+ laser lying in the (110) plane are incident upon the $(\bar{1}10)$ face of the sample. In order to optimize the two-wave mixing gain and to minimize the output intensity oscillations due to the electrically induced changes of the birefringence (and therefore of the photorefractive gain), the incident beams are linearly polarized along the [110] axis.[10] The induced index modulation leads to an energy redistribution between the two input beams, the probe and the pump. If the pump beam intensity is much larger than the probe beam intensity, then the probe beam intensity I_p in the presence of the pump beam is related to the probe beam intensity I_a in the absence of the pump beam by[3]

$$I_p = I_a e^{gL}, \tag{14}$$

where L is the interaction length and g is the photorefractive gain proportional to the imaginary part of the space-charge field δE. Thus the kinetics of δE can be observed by monitoring I_p.

MOBILITY MEASUREMENTS

The main advantage of the square-wave technique is that we can rely on Eqs. (7) and (9) to describe the observed phenomenon and to deduce the exact value of the mobility. During each half-period of the ac field, the electric field is indeed constant. This is no longer true with the second method, which uses a sinusoidal field. Equation (2) is indeed no longer valid for a continuously time-dependent applied electric field. Consequently we will use the square-wave method first, and a comparison of the results obtained employing the second technique will give us a proof of the validity of the sinusoidal field technique.

The first sample that we study is a Fe-doped BGO crystal (hereafter termed BGO 1) grown at the Université de Bordeaux, France. Its dimensions are 4.1 mm × 6.6 mm × 7.9 mm along the [001], [110], and $[\bar{1}10]$ axes. The pump intensity (I = 960 μW/cm^2 at wavelength λ = 488 nm) is 400 times larger than the probe beam intensity. For this optical irradiance we checked that the slow time constant τ_b (a few seconds) is much larger than the fast time constant so that the expression for τ_a given by Eq. (4) is valid. The fringe spacing Λ of the photoinduced grating is 61 ± 2 μm.

In Fig. 1 we have plotted the amplified probe beam intensity versus time for a square-wave applied field (peak voltage 1.5 kV for an electrode spacing of 4.1 mm, two-wave mixing gain g = 1.4 cm^{-1}). This figure clearly shows the damped oscillations of the amplified intensity

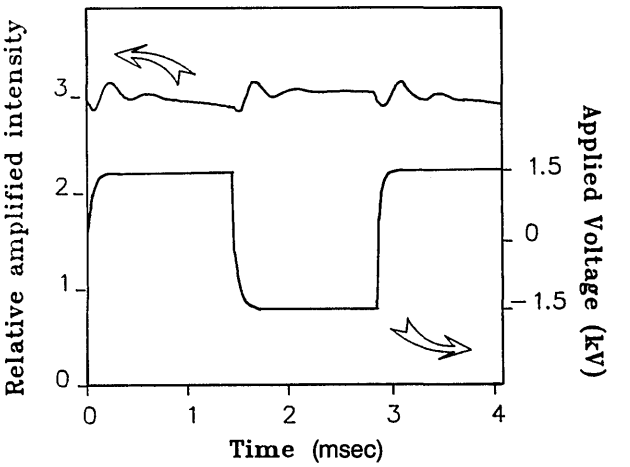

Fig. 1. Kinetics of the relative amplified intensity (output probe beam intensity with pump beam on/output probe beam intensity with pump beam turned off) and the corresponding applied voltage.

after each switch of the applied field. According to Eq. (2), the oscillation frequency is $1/2\pi\tau_E$. Therefore from Eq. (5) we get

$$\frac{\Lambda}{|\mu|E_0} = 375 \pm 30\ \mu\text{sec}. \tag{15}$$

This period $2\pi\tau_E$ represents the time needed for the charge carriers to travel from one fringe to another one. The oscillations shown in Fig. 1 can be interpreted as follows. The period T of the ac field is larger than τ_a but slower than τ_b. Thus, before each switch of the ac field, the charge-carrier grating is in equilibrium under the influence of both the applied field and the ionic grating space-charge field. After the sudden change in the value of E_0, the charge-carrier grating migrates at a velocity μE_0. The beating of this moving modulation with the quasi-static ionic grating (which builds up from charge-carrier recombination) produces the oscillating behavior of the gain. This explanation demonstrates that the observed phenomenon does not depend on the quasi-static band-transport model that we have used in this paper to determine the best experimental conditions.

The same physical explanation holds to describe the origin of the resonance frequency that appears when a two-beam coupling experiment is performed under a sinusoidal electric field. In Fig. 2 we show the photorefractive gain versus the applied field frequency. The peak value of the sinusoidal field is 1.5 kV, and the other experimental conditions remain unchanged (Λ = 61 ± 2 μm, I = 960 μW/cm^2, λ = 488 nm). The resonance peak at ν_{res} = 1200 ± 30 Hz is explained as follows. When the applied field is close to zero, a charge-carrier grating builds up in phase with the interference pattern. During the positive (or negative) phase of the applied field, these charge carriers are shifted by a length d:

$$d \simeq \int_0^{T/2} |\mu| E_0 \sin\left(\frac{2\pi}{T}t\right) dt \tag{16}$$

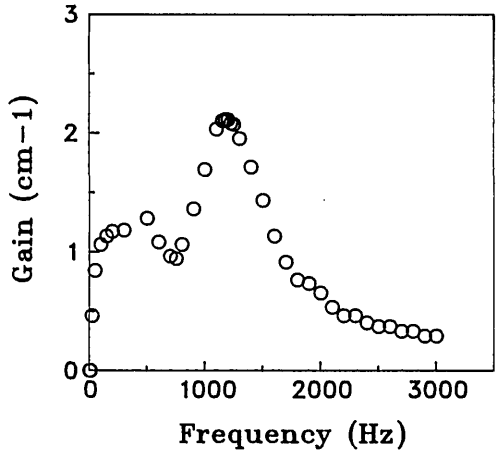

Fig. 2. Photorefractive two-wave mixing gain versus the frequency of the sinusoidal applied electric field for BGO 1 (see text). The resonance peak is located at $\nu_{res} = 1200$ Hz.

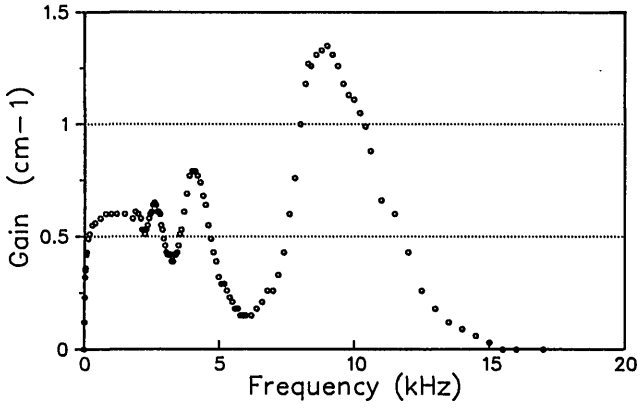

Fig. 3. Photorefractive two-wave mixing gain for BGO 2 (see text) versus the frequency of the sinusoidal applied field. Four resonance and four antiresonance frequencies are visible.

and then recombine mostly at this length d. During the other phase of the applied field, the same process occurs. If the drift length d is equal to an odd number of half-fringe spacings $\Lambda/2$, then the charge carriers recombine mainly in the dark fringes. The buildup of the photorefractive grating is thus optimized for two-beam coupling. Conversely, if d is a multiple of Λ, then the photorefractive grating is reduced. In Fig. 2 we see only the main resonance frequency (for $d = \Lambda/2$) and one antiresonance frequency (for $d = \Lambda$). However, for one sample (which we term BGO 2) we have observed four different resonance frequencies (for $d = \Lambda/2, 3\Lambda/2, 5\Lambda/2, 7\Lambda/2$) and other four antiresonance frequencies (for $d = \Lambda, 2\Lambda, 3\Lambda, 4\Lambda$), as shown in Fig. 3. From inequality (16) we calculate the main resonance frequency:

$$\nu_{res} \simeq \frac{2|\mu|E_0}{\pi\Lambda}. \tag{17}$$

From the curve in Fig. 2 we get

$$\frac{\Lambda}{|\mu|E_0} \simeq \frac{2}{\pi\nu_{res}} = 530 \pm 15\ \mu\text{sec}. \tag{18}$$

This value [relation (18)] is slightly larger than the one measured previously [Eq. (15)] with the square-wave field method. The reason is that some charge carriers recombine before the end of the half phase of the ac field. Thus inequality overestimates the length d. The agreement between the two methods is better when several frequencies are visible and the measurement is achieved by taking into account the lowest resonant frequency (for $d = n\Lambda/2$ with n maximum).

According to the physical explanation of this resonance peak, at the main resonance frequency the charge-carrier grating passes over the dark (or bright) fringes twice during each period T. Consequently, for this special frequency the photorefractive gain should have a component oscillating at twice the frequency ν_{res}. This phenomenon is clearly visible in Fig. 4, which shows the kinetics of the amplified beam for ν_{res}.

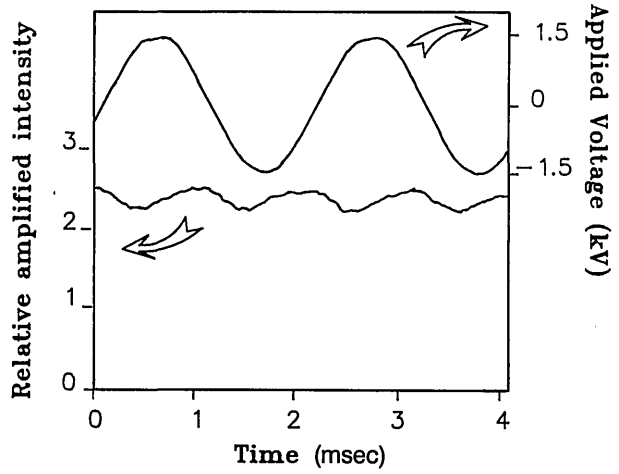

Fig. 4. Relative amplified intensity versus time at the resonance frequency ν_{res}. All the experimental conditions are the same as for Fig. 2. The intensity oscillates at twice the applied voltage frequency ν_{res}.

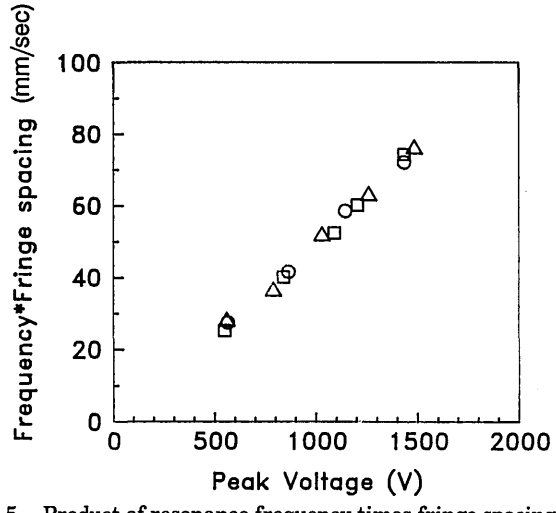

Fig. 5. Product of resonance frequency times fringe spacing versus the peak voltage of the applied sinusoidal electric field. Squares correspond to the fringe spacing $\Lambda = 18$ μm and to the optical wavelength $\lambda = 514$ nm; circles correspond to $\Lambda = 30$ μm and $\lambda = 514$ nm; triangles correspond to $\Lambda = 29$ μm and $\lambda = 488$ nm.

Table 1. Summary of Measurements Performed on Three BGO Samples with Different Dopings with the Square-Wave and the Sinusoidal Field Methods

Sample	Mobility		Recombination Time (μsec)	L (μm)	
	Square-Wave Method [10^{-6} m^2/(V-sec)]	Sinusoidal Method		Square-Wave Method	Sinusoidal Method
BGO 1 (Fe)	0.44	0.32	1200	3.7	3.2
BGO 2 (Fe)	1.8	1.3	525	4.9	4.2
BGO 3 (Fe + V)	0.70	0.44	650	3.4	2.7

In order to prove definitively that the resonance frequency is related to the mobility by formula (17), we measured, for various fringe spacings, optical wavelengths (λ = 488 or 514 nm), and applied voltages V the product $\nu_{res}\Lambda$ versus V. The experimental data are shown in Fig. 5. The measurements at wavelength λ = 515 nm are represented by squares for a fringe spacing $\Lambda = 18.3 \pm 0.5$ μm and by circles for a fringe spacing $\Lambda = 30.3 \pm 1.5$ μm. Triangles correspond to measurements performed at λ = 488 nm and $\Lambda = 28.8 \pm 1.5$ μm. All these data are aligned on a straight line passing through the origin, as predicted by formula (17). This also means, first, that the mobility does not depend on the applied voltage and, second, that the electric field E_0 is proportional to the applied voltage. We assume that the applied electric field is related to this voltage and to the electrode spacing d by

$$E_0 = V/d. \tag{19}$$

We also checked that the resonance frequencies do not depend on the optical irradiance. However, the amplitude of the two-wave mixing gain at these resonant frequencies depends on the irradiance and can be larger or smaller than the two-wave mixing gain obtained with a square-wave applied field. For instance, for BGO 1 and for the same experimental conditions (λ = 488 nm, I = 980 μW/cm^2, Λ = 61 μm), the maximum two-wave mixing gain with a sinusoidal applied field (g = 2.1 cm^{-1} in Fig. 2) is larger than the gain obtained with a square-wave applied field (g = 1.4 cm^{-1} in Fig. 1).

DISCUSSION

Results of measurements for three different BGO samples grown by the Czochralski method at the Université de Bordeaux are listed in Table 1. The Fe concentration in the melt was 50 parts in 10^6 for BGO 1 and 17 parts in 10^6 for BGO 2. For the Fe + V-doped BGO 3, the Fe concentration was 22 parts in 10^6 and the V concentration 20 parts in 10^6.

The second column in Table 1 shows the absolute values of the mobility determined by using the square-wave method. The uncertainties are ~10%. More-precise measurements are easily achievable. However, we have experimentally observed that the measured values were a little bit higher (a few percent) when the sample was heated by Joule's effect. Therefore more-accurate measurements will be significant only with a temperature-stabilized setup. The next column shows the measured absolute values for the mobility obtained by using the sinusoidal field technique and performing the calculation on the main resonance peak. In these experiments there is a systematic error due to the use of the approximate formula (17). This error is difficult to evaluate. However, it can be minimized by performing the measurements on the other resonance peaks as explained above. The values for the recombination time constants listed in the fourth column are obtained by measuring the exponential decay of the photocurrent when the illuminating beams are turned off. These values are much larger than usual ones, and this is a function of the choice of the BGO samples. Indeed, owing to the limited frequency bandwidth of our ac field power supply, we were able to perform measurements only on those special samples because of the condition that $\tau_E \ll \tau_R$. The only samples with large recombination time constants were Fe doped. This is not merely a coincidence, as Table 1 shows: the more heavily doped the sample, the longer the recombination time constant and the smaller the mobility. The diffusion lengths, in the fifth and sixth columns, are calculated by reporting the values for the mobilities and recombination time constants in Eq. (1). The uncertainties on L obtained with the square-wave method are ~10%. For the sinusoidal method, the uncertainties are again more difficult to evaluate; however, the agreement between the two methods is satisfactory.

CONCLUSION

We have presented two techniques to measure photocarrier mobilities. In the first one, the square-wave technique, the mobility is deduced from the kinetics of the two-wave mixing gain; in the second, the mobility is derived from the gain magnitude when a sinusoidal field is employed. The square-wave technique can produce highly accurate measurements. However, the photorefractive sample must be thermally stabilized. The sinusoidal field method is less accurate but easier to perform because the requirement on the frequency bandwidth of the electric power supply is not so strong. Nevertheless, this method is precise enough to permit different samples to be classified according to the mobility values.

We employed both methods to study three Fe-doped BGO samples. We observed that the heavier the doping, the smaller the mobility and the larger the recombination time, so the diffusion lengths for all three samples are similar.

REFERENCES

1. P. Günter and J. P. Huignard, *Photorefractive Materials and Their Applications II,* Vol. 62 of Topics in Applied Physics (Springer-Verlag, Berlin, 1989).

2. P. Yeh, A. E. Chiou, J. Hong, P. Beckwith, T. Chang, and M. Khoshevisan, Opt. Eng. **28,** 328 (1989).
3. N. V. Kukhtarev, V. B. Markov, S. G. Odulov, M. S. Soskin, and V. L. Vinetskii, Ferroelectrics **22,** 949 (1979).
4. J. M. C. Jonathan, R. W. Hellwarth, and G. Roosen, J. Opt. Soc. Am. A **1,** 1245 (1984).
5. R. A. Mullen and R. W. Hellwarth, J. Appl. Phys. **58,** 40 (1985).
6. G. Pauliat, J. M. C. Jonathan, M. Allain, J. C. Launay, and G. Roosen, Opt. Commun. **59,** 266 (1986).
7. G. C. Valley, IEEE J. Quantum Electron. **QE-19,** 1637 (1983).
8. S. I. Stepanov and M. P. Petrov, Opt. Commun. **53,** 292 (1985).
9. C. Besson, J. M. C. Jonathan, A. Villing, G. Pauliat, and G. Roosen, Accepted for publication in Optics Letters.
10. G. Pauliat, C. Besson, and G. Roosen, IEEE J. Quantum Electron. **25,** 1736 (1989).